Available online at www.sciencedirect.com
ScienceDirect
Journal of Solid State Chemistry 181 (2008) 175–182
JOURNAL OF SOLID STATE CHEMISTRY
www.elsevier.com/locate/jssc

Preparation and photoelectrocatalytic activity of a nano-structured WO_3 platelet film

Masayuki Yagi[a,*], Syou Maruyama[a], Koji Sone[a], Keiji Nagai[b], Takayoshi Norimatsu[b]

[a]*Faculty of Education and Human Sciences, Center for Transdisciplinary Research, Niigata University, 8050 Ikarashi-2, Niigata 950-2181, Japan*
[b]*Institute of Laser Engineering (ILE), Osaka University, 2-6 Yamada-Oka, Suita, Osaka 565-0871, Japan*

Received 27 August 2007; received in revised form 10 November 2007; accepted 16 November 2007
Available online 22 November 2007

Abstract

A tungsten trioxide (WO_3) film was prepared by calcination from a precursor paste including suspended ammonium tungstate and polyethylene glycol (PEG). The ammonium tungstate suspension was yielded by an acid–base reaction of tungstic acid and an ammonium solution followed by deposition with ethanol addition. Thermogravimetric (TG) analysis showed that the TG profile of PEG is significantly influenced by deposited ammonium tungstate, suggesting that PEG is interacting strongly with deposited ammonium tungstate in the suspension paste. X-ray diffraction (XRD) data indicated that the WO_3 film is crystallized by sintering over 400 °C. The scanning electron microscopic (SEM) measurement showed that the film is composed of the nano-structured WO_3 platelets. The semiconductor properties of the film were examined by Mott–Schottky analysis to give flat band potential $E_{FB} = 0.30$ V vs. saturated calomel reference electrode (SCE) and donor carrier density $N_D = 2.5 \times 10^{22}\,cm^{-3}$, latter of which is higher than previous WO_3 films by two orders of magnitude. The higher N_D was explained by the large interfacial heterojunction area caused by the nano-platelet structure, which apparently increases capacitance per a unit electrode area. The WO_3 film sintered at 550 °C produced 3.7 mA cm^{-2} of a photoanodic current at 1.2 V vs. SCE under illumination with a 500 W xenon lamp due to catalytic water oxidation. This photocurrent was 4.5–12.8 times higher than those for the other control WO_3 films prepared by similar but different procedures. The high catalytic activity could be explained by the nano-platelet structure. The photocurrent was generated on illumination of UV and visible light below 470 nm, and the maximum incident photon-to-current conversion efficiency (IPCE) was 47% at 320 nm at 1.2 V. Technically important procedures for preparation of nano-structured platelets were discussed.

Keywords: Tungsten trioxide; Photoelectrocatalysis; Platelet film; Water oxidation

1. Introduction

Design and development of nano-structured materials have expanded new research fields of materials and surface sciences since ''nanotechnology'' was propounded at the end of the last century [1,2]. Metal oxide semiconductors have been extensively studied for its fundamental science and a wide variety of application to photocatalysts, displays, batteries and solar cells [3–8]. Titanium oxide (TiO_2) is one of the semiconductors that have been studied most actively due to its attractive photocatalytic activities [6] without photocorrosion and its successful application to dye-sensitized solar cells [7,8]. Nano-crystalline TiO_2 is effective for a large surface area with high crystallinity kept, giving high photocatalytic activities. A nano-structured interfacial heterojunction between TiO_2 and an electrolyte solution is also important for dye adsorption and light harvest in dye-sensitized solar cells.

Since TiO_2 exhibits photocatalytic activity in being exposed to ultraviolet (UV) light (>3.1 eV), TiO_2 has a disadvantage for converting visible light in solar light from the viewpoint of practical solar energy application. Tungsten trioxide (WO_3) is also an n-type semiconductor possessing a resistance to photocorrosion and a photocatalytic activity in acidic conditions. WO_3 has a more advantage for solar energy utilization than that of TiO_2 because the band gap energy (2.5–2.7 eV) of the former is

*Corresponding author. Fax: +81 25 262 7151.
E-mail address: yagi@ed.niigata-u.ac.jp (M. Yagi).

0022-4596/$ - see front matter © 2007 Elsevier Inc. All rights reserved.
doi:10.1016/j.jssc.2007.11.018

lower than that of the latter. However, the photocatalytic and photoelectrochemical characteristics of WO_3 have not been studied as extensively as those of TiO_2.

WO_3 films have been prepared by several techniques, e.g., vacuum evaporation [9], chemical vapor deposition [10,11], sol–gel precipitation [12–15], spin coating [16], sputtering [17] and electrodeposition [18–22]. Although a sol–gel technique is one of the simple and low-cost procedures selected for a wide range of applications, there have been only a few reports on photoelectrochemical characteristics of the WO_3 film prepared by a sol–gel technique [12–15]. In previous procedure by a sol–gel technique, the precursor (tungstic acid) was obtained by passing an aqueous solution of sodium tungstate through a column filled with a proton exchange resin, followed by adding PEG to the solution to give viscous precursor solution. It was cast on a substrate and then annealed under oxygen atmosphere at 550 °C. Herein, we report that a WO_3 film composed of a nano-structured platelet is prepared by a simpler and easier procedure (without a cation exchange procedure) and that it produces a significant photoanodic current of a milliampere order under illumination with a 500 W xenon lamp due to catalytic water oxidation. The preparation and photoelectrocatalytic activity of the nano-structured WO_3 platelet film will be discussed.

2. Experimental

2.1. Materials

The purest grades of tungstic acid, ammonium tungstate pentahydrate (Kanto Chemical Co. Inc.), ammonia aqueous solution (Junsei Chemical Co., Ltd.), and polyethylene glycol (PEG) ($M_w = 20.000$, Wako Pure Chemical Ind., Ltd.) were purchased and used as received. An indium tin oxide (ITO)-coated glass with 10 Ω/sq of a sheet resistance was purchased from Kinoene Kogaku Kogyo Co., Ltd.

2.2. Preparations

Tungstic acid (yellow powder; 0.25 g, 1.0 mmol) was dissolved in a 30% ammonia aqueous solution (0.6 ml) to give a colorless solution containing a little bit of white precipitate (ammonium tungstate). Ethanol (1.0 ml) and PEG (0.78 g) were added to the solution, providing the viscous stable suspension of ammonium tungstate as a precursor paste. It was squeegeed on the ITO substrate by means of a doctor blade technique using scotch tape as a spacer, and then air-dried for 30 min followed by a calcination treatment at 300–550 °C for 90 min to form a WO_3 film. This film was abbreviated to the type-A film to distinguish from the other control film of types—B, C and D. For the type-B film, the same amount of tungstic acid (0.25 g, 1.0 mmol) was suspended in water (0.6 ml), and then ethanol (1.0 ml) and PEG (0.78 g) were added to obtain a precursor paste. For the type-C film, the same amount of tungstic acid (0.25 g, 1.0 mmol) was dissolved in a 30% ammonia aqueous solution (0.6 ml), and then PEG (0.78 g) was added without addition of ethanol to obtain a precursor paste. For the type-D film, commercially available ammonium tungstate was suspended in water (0.6 ml) and then ethanol (1.0 ml) and PEG (0.78 g) were added to obtain a precursor paste. For all the films of type—A–D, the precursor pastes were conditioned for tungsten atom concentration (0.63 mmol/ml) to be constant before the squeegee. The type-B, C and D films were formed from respective precursor pastes by the same calcination treatment as the type-A film.

2.3. Measurements

Thermogravimetric (TG) data were taken at 10 °C min^{-1} using a TG analyzer (Shimadzu, DTG-60). XRD data were recorded using an X-ray diffractometer (MAC Science, MX labo). SEM measurements were carried out using a scanning electron microscope (JEOL JSM-7400F) operated at an accelerating voltage of 2 kV. UV–visible diffuse reflectance (DR) spectra were measured using a UV–visible spectrophotometer (JASCO V-550) in a DR mode. Electrochemical experiments were conducted in a single compartment electrochemical cell equipped with the WO_3 film-coated ITO working electrode, a saturated calomel reference electrode (SCE) and a platinum wire counter electrode using an electrochemical analyzer (Hokuto Denko, HZ-3000). The capacitance was given at 45 mHz of a frequency and 10 mV of amplitude potential in alternating-current impedance measurements using the electrochemical analyzer interfaced with a frequency response analyzer (NF Electronic Instruments, S-5720c). A 500 W xenon lamp (Ushio, UXL-500SX) in a lamp house (SX-U1500XG) was used for photoelectrochemical measurements. A monochromic light with 8 nm of a bandwidth was given from the 500 W xenon lamp using a monochromator. All the electrochemical and photoelectrochemical experiments were carried out under argon atmosphere at 25 °C.

3. Results and discussion

Tungstic acid reacts with an ammonia aqueous solution to give a colorless ammonium tungstate solution. The titration of a 30% ammonia aqueous solution to the tungstic acid (1.0 mmol) showed that 0.6 ml (9.5 mmol) of the ammonia aqueous solution is required to give an ammonium tungstate solution by an acid–base reaction. The addition of ethanol to the ammonium tungstate solution yielded fine white deposit, which precipitates for a few minutes in the solution. However, in the presence of PEG, it dispersed stably in a suspension paste for at least a few weeks. Instead of PEG, ethylene glycol, glycerol and mannitol were used for preparation of suspension pastes. The paste using ethylene glycol or glycerol was inappropriate for squeegee on an ITO glass, whereas the paste using

PEG or mannitol was uniformly squeegeed on the ITO glass. Since the photoelectrocatalytic activity (*vide infra*) of the WO_3 film prepared from the paste using PEG was however higher than that of the paste using mannitol by a factor of 2–3, the study was focused on the WO_3 film prepared from the paste using PEG.

TG analysis was carried out to examine thermochemical characters of the fine white deposit formed in the suspension paste using PEG. The TG curve of the air-dried residual solid from the suspension solution containing deposited ammonium tungstate (without PEG) is shown in Fig. 1a. The gravity fraction gradually decreased with a temperature increase from room temperature to 550 °C, and the total gravity decrease was 12.7%. This is roughly close to the theoretical gravity decrease (18.3%) in pyrolysis of $(NH_4)_2WO_4$ according to Eq (1).

$$(NH_4)_2WO_4 \xrightarrow{heat} WO_3 + 2NH_3 + H_2O. \quad (1)$$

Pyrolysis of PEG occurred monotonically at 300–400 °C with 100% decrease of the gravity fraction, as shown in Fig. 1b. However, the gravity fraction of the air-dried residual solid from the suspension paste containing deposited ammonium tungstate with PEG was initiated to decrease at 250 °C with two pyrolytic phases up to 400 °C, and the total decrease of the gravity fraction was 83.8% up to 550 °C (Fig. 1c). This fraction is consistent with the total content (78.2%) of PEG in the residual solid as well as NH_3 and water evolved stoichiometrically by pyrolysis of ammonium tungstate in Eq (1). The TG profile of deposited ammonium tungstate with PEG (Fig. 1c) is different from those of deposited ammonium tungstate (without PEG) and PEG either alone or in combination. This result suggests that the deposited ammonium tungstate is interacting significantly with PEG in the suspension paste. The interaction could be important for stabilization of the suspension paste by PEG.

The WO_3 film was obtained by air-dry followed by a calcination treatment of the squeegeed suspension paste on the ITO substrate. The thickness of the WO_3 film was 30 μm under the typical conditions as measured by SEM measurements. XRD data of the WO_3 films sintered at various temperatures at 300–550 °C are shown in Fig. 2. It did not show any peaks except for the ITO substrate below 350 °C, indicating amorphous WO_3 under the conditions. However, it exhibited sharp and intense peaks for crystallinity of WO_3 at higher temperatures than 400 °C, showing that WO_3 is crystallized over 400 °C. The XRD diffraction pattern of the film suggests monoclinic structure in a main phase of WO_3 film. The SEM image (× 5000) of the surface of the WO_3 film sintered at 550 °C showed a porous structure, and the magnification (× 30000) visualized nano-structured WO_3 platelets, as shown in Fig. 3. The significant difference in the SEM data were not observed among the film sintered 450–550 °C, but a lump structure (not nano-structured platelets) was seen as sintered at 350 °C. This reveals that calcination over 450 °C is required for formation of nano-structured platelets.

Alternating-current impedance measurements were conducted to evaluate the semiconductor characters for the WO_3 film. The capacitance ($C/F\,cm^{-2}$) is related to

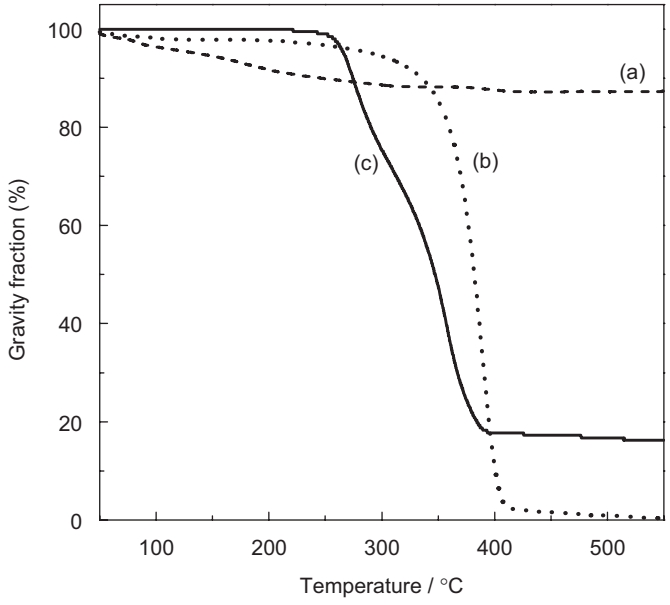

Fig. 1. Thermogravimetric curves of (a) deposited ammonium tungstate, (b) PEG and (c) deposited ammonium tungstate with PEG.

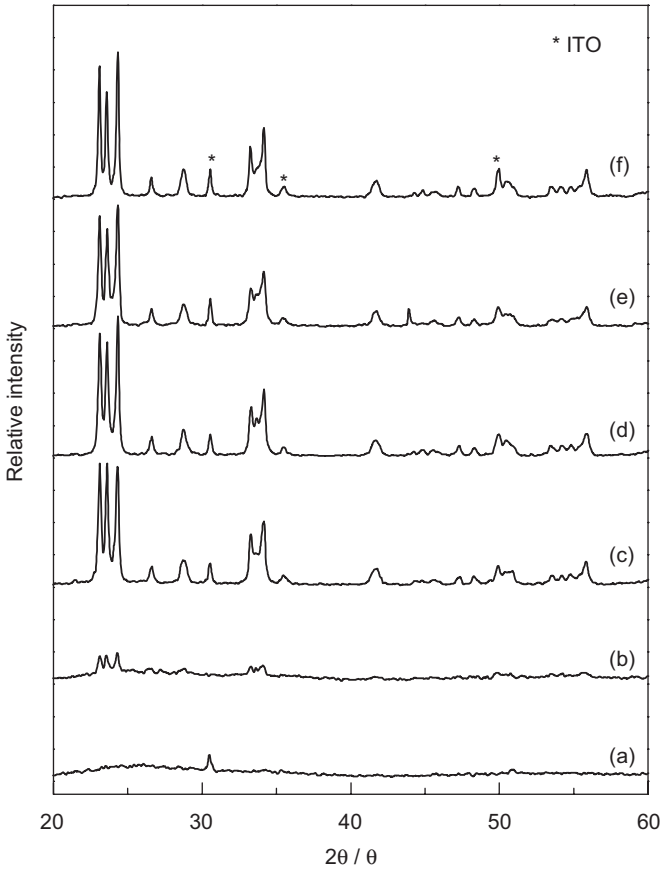

Fig. 2. XRD patterns of the type-A WO_3 film sintered at (a) 300, (b) 350, (c) 400, (d) 450, (e) 500 and (f) 550 °C.

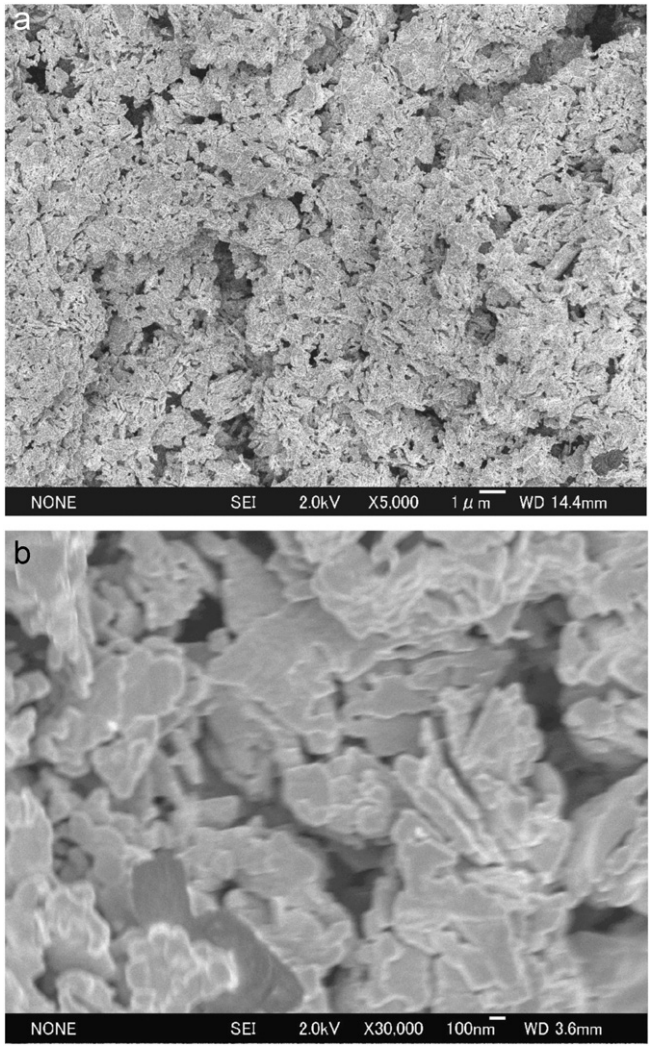

Fig. 3. SEM images at the surface of the type-A WO_3 film sintered at 550 °C (a) × 5000 and (b) × 30000.

the applied potential (E/V) by the Mott–Schottky equation (Eq (2)),

$$\frac{1}{C^2} = \left(\frac{2}{q\varepsilon\varepsilon_0 N_D}\right)\left(E - E_{FB} - \frac{kT}{q}\right), \quad (2)$$

where q is the electronic charge, ε is the relative permittivity (50 for WO_3) [23] of the semiconductor, ε_0 is the vacuum permittivity (8.85×10^{-14} F cm^{-1}), N_D/cm^{-3} is the donor carrier density, E_{FB}/V is the flat band potential of the semiconductor, k is the Boltzmann constant, T/K is the absolute temperature, respectively. The plots of C^{-2} vs. E gave a straight line above 0.4 V, as shown in Fig. 4. The E_{FB} and N_D values were provided from the x-intercept and the slope of the straight line to be $E_{FB} = 0.30$ V vs. SCE and $N_D = 2.5 \times 10^{22}$ cm^{-3}, respectively. The E_{FB} is close to the earlier-reported data (0.35 V vs. SCE) for a spray deposited WO_3 film from an ammonium tungstate solution [11]. The N_D values of the spray deposited WO_3 film and a WO_3 particle film prepared by a heat treatment from a WO_3 sol were reported to be $N_D = 1.5 \times 10^{20}$ cm^{-3} [11] in

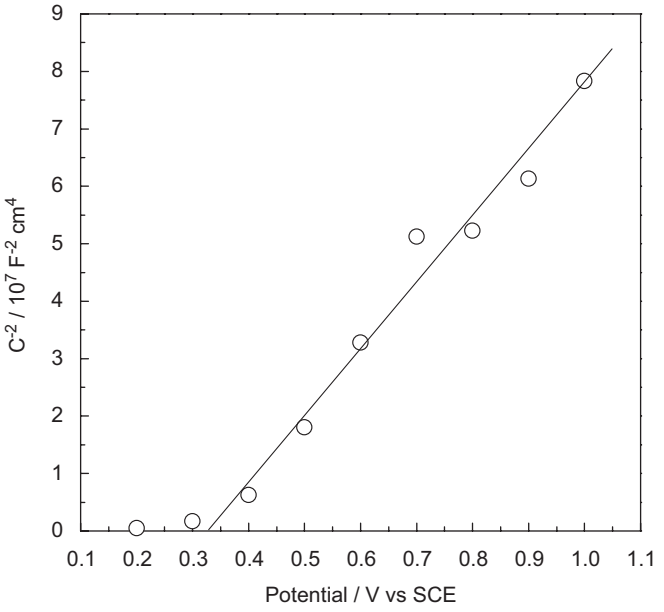

Fig. 4. Mott–Schottky plot of the type-A WO_3 film sintered at 550 °C. The capacitance was measured at 45 mHz of a frequency and 10 mV of amplitude potential.

a 0.1 M Na_2SO_4 aqueous solution and $N_D = 1 \times 10^{20}$ cm^{-3} [24] in an aqueous solution containing 0.3 M oxalic acid and 0.5 M Na_2SO_4, respectively. The N_D values are $1–2 \times 10^{20}$ cm^{-3} in other WO_3 films reported previously to our knowledge [11,24–26]. The N_D (2.5×10^{22} cm^{-3}) for the present WO_3 film was higher than the previous data by two orders of magnitude. The high N_D value (2.5×10^{22} cm^{-3}) of the WO_3 film could be explained by the large interfacial heterojunction area. It could apparently increase the capacitance (ascribed to a space charge layer) per a unit electrode area.

Cyclic voltammogram (CV) of the present WO_3 film in a 1.0 M $HClO_4$ aqueous solution is shown in Fig. 5a under the dark conditions. Although the redox response of H_xWO_3/WO_3 was observed below 0.3 V, the anodic current was hardly observed in the range of 0.3–1.5 V owing to an n-type Schottky barrier at an interfacial heterojunction between the film surface and the electrolyte solution. Light irradiation to the film significantly induced the anodic current due to water oxidation over 0.35 V that is nearly the same as E_{FB} (0.30 V) of the WO_3 film, and it reached 4.4 mA cm^{-2} at 1.5 V, as shown in Fig. 5b. The photoanodic current at 1.5 V on CV increased linearly from 0.58 to 4.4 mA cm^{-2} with an increase of the film thickness from 5.7 to 30 μm, implying that the interior site closed to the interface of the film/ITO as well as the film surface is effective for photocurrent generation under the conditions employed.

To reveal the influence of the sintering temperature on the photoelectrocatalytic activity, the photocurrents were measured using the WO_3 films sintered at different temperatures of 350–550 °C. The photocurrent was not generated on the film sintered at 350 °C but generated

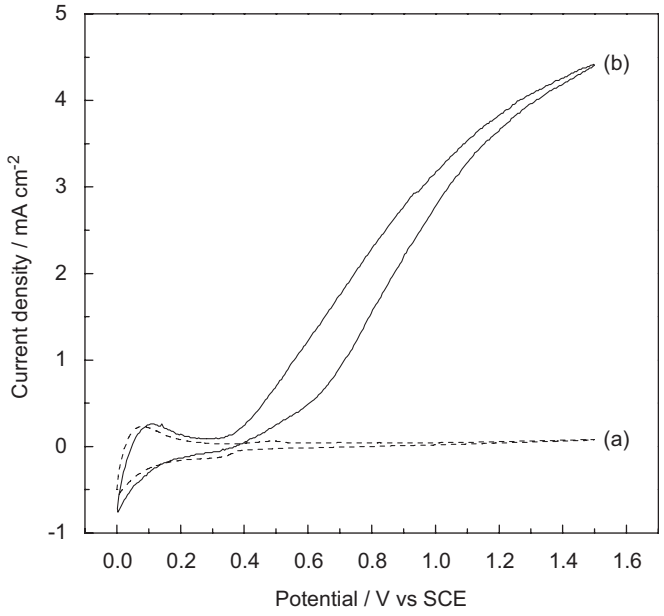

Fig. 5. Cyclic voltammograms of the type-A WO_3 film (sintered at 550 °C) in a 1.0 M $HClO_4$ aqueous solution (a) under dark and (b) illumination.

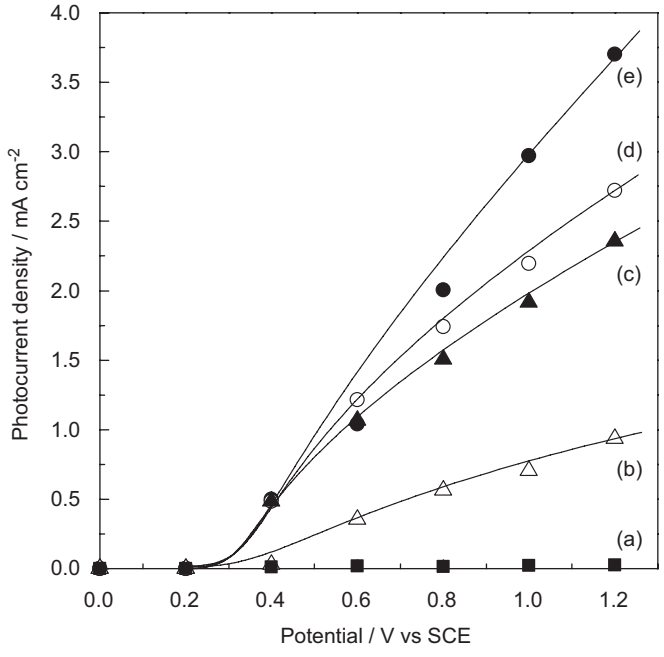

Fig. 6. Plots of photocurrent vs. applied potential for the type-A WO_3 film sintered at (a) 350, (b) 400, (c) 450, (d) 500 and (e) 550 °C.

significantly by sintering over 400 °C, as shown in Fig. 6. This is consistent with crystallization of WO_3 by sintering over 400 °C, suggested by the XRD data (Fig. 2). This indicates that crystallinity of the WO_3 film is of importance for the catalytic activity. The photocurrent for the film sintered at 400 °C was lower than those sintered at 450–550 °C when comparing at 0.4 V although the XRD data are almost the same in calcination at 400–550 °C. Amorphous WO_3 films are known to characteristically give the higher electroactivity of the H_xWO_3/WO_3 redox (below 0.3 V) than those for crystalline WO_3 films on the CV. The corresponding redox responses on the present WO_3 films sintered at 300–400 °C were significantly higher than those sintered at 450–550 °C, suggesting that the film sintered at 400 °C partially includes amorphous WO_3. This is supposed to be responsible for the lower photocurrent at 400 °C. The XRD and CV data indicate that the calcination at 400 °C for 90 min is critical conditions to produce a crystalline WO_3 film.

The photocurrent at 1.2 V increased with an increase in the sintering temperature from 450 to 550 °C by a factor of 1.6 although the photocurrents below 0.6 V were nearly the same. The photocurrent is based on water oxidation by photogenerated holes that competed with recombination with electrons. Since the recombination is supposed to be a predominant process at low applied potentials, nearly the same photocurrent below 0.6 V suggests that the degree of the recombination does not depend on the sintering temperature of 450–550 °C. As the applied potential increases, the photocurrent should increase because of the decreased degree of recombination, and thereafter saturate at sufficiently high-applied potentials when it is negligibly low. The photocurrent at higher potentials should be influenced in principle by the catalytic reaction at the surface, rather than the degree of recombination. The higher photocurrent at higher potentials (above 0.8 V) for the 550 °C-sintered film can be explained by the increased catalytic activity of the surface. Most possibly, the surface could be activated by sintering at 550 °C due to removal of the adhesive cinders of PEG out of the surface. This is supported by the slight but distinguished decrease of the gravity fraction in the range of 450–550 °C in the TG profile (Fig. 1c).

The photocurrent at 1.2 V was measured with changing wavelength of illumination monochromic light. The photocurrent was observed in a UV and visible light region below 470 nm, and the maximum IPCE was 47% at 320 nm. An action spectrum of IPCE was consistent with the UV–visible DR spectrum of the film (with an absorption edge at 470 nm), as shown in Fig. 7, corroborating that the photocurrent is based on a band gap photoexcitation of WO_3. It causes holes and electrons to be generated, and the former oxidizes water at the surface, the latter reducing proton at a counter electrode surface.

To examine products for water oxidation on the film, the photoelectrocatalysis was preliminary performed at 0.6 V for 60 min. The gas in a headspace of a gas-tight reaction cell was analyzed using a gas chromatograph. 2.6 μmol of O_2 was detected as a 4-electron oxidized product from water. However, the faraday efficiency (30%) for O_2 production was lower than that (78%) for H_2 production at the counter electrode (13.5 μmol of H_2 was detected together with O_2). The formation of hydrogen peroxide might be possible as an explanation of the lower yield of O_2. However, Augustynski's et al. [15] reported that the faraday efficiency of hydrogen peroxide is ca. 5% on their WO_3 film in a 1.0 M $HClO_4$ solution under simulated solar

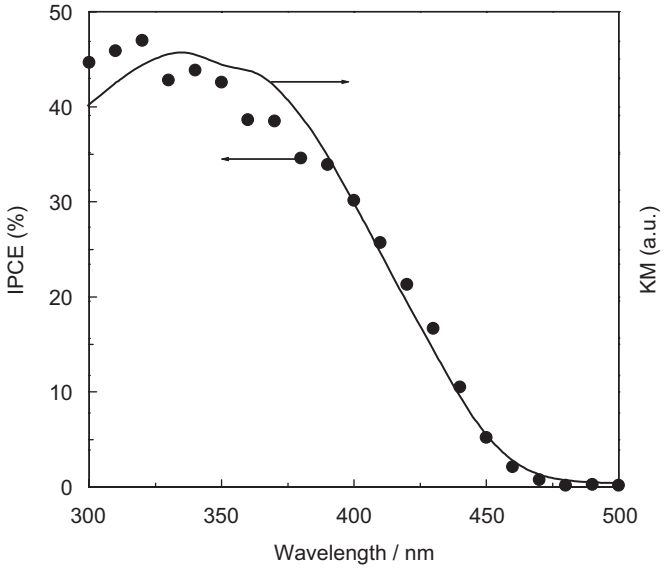

Fig. 7. Action spectrum (plot) of IPCE and UV–visible DR spectrum (solid line) of the type-A WO_3 film sintered at 550 °C. IPCE was measured in a 1.0 M $HClO_4$ aqueous solution at 1.2 V vs. SCE.

AM 1.5 illumination. Leaustic et al. [27] reported clear evidence for formation of hydroxyl radical in suspension of WO_3 powder under illumination by a radical-trapping technique. In the present photoelectrocatalysis, it is most likely that hydroxyl radicals are bound on the film surface as radical adducts, or they are coupled with each other to form peroxide adduct bound on the surface.

Now we compare the present WO_3 film (abbreviated to the type-A film) with three different types of control WO_3 films prepared by the similar method to the type-A film: (1) the type-B film prepared from tungstic acid without an ammonia solution, (2) the type-C film prepared without addition of ethanol for deposition, (3) the type-D film prepared from commercially available ammonium tungstate (see Table 1). Augustynski's group reported that a mesoporous WO_3 film consisting of preferentially orientated monoclinic-phase nano-crystals is prepared from an aqueous tungstic acid solution obtained by proton exchange of a sodium tungstate solution [12,14,15]. We tried preparing their WO_3 film as a control, but the appearance of the film was not uniform because the precursor solution is repelled on the ITO electrode. It did not exhibit preferentially orientated monoclinic-phase crystals of WO_3 on its XRD data. The unsuccessful preparation might be caused by the difference from either the transparent oxide conductive substrate (The FTO substrate was used in their preparation), or the treatment procedure of the substrate surface for their preparation.

The photocurrent was measured at 1.2 V under the same WO_3 amount conditions to compare the catalytic activity of type—A–D films. No significant difference in the electroactivity of WO_3 among these films was corroborated by nearly the same anodic peak currents (within a 15% error) at 0.1 V based on the H_xWO_3/WO_3 redox in CV data. Time profiles of the photocurrent responses by

Table 1
Summary of photocurrent densities at various films at 1.2 V

WO_3 film	Photocurrent density/ mA cm^{-2}
Type-A	3.7
Type-B (without reaction with NH_3)	0.83
Type-C (without ethanol addition)	0.29
Type-D (using commercially available $(NH_4)_2WO_4$)	0.67

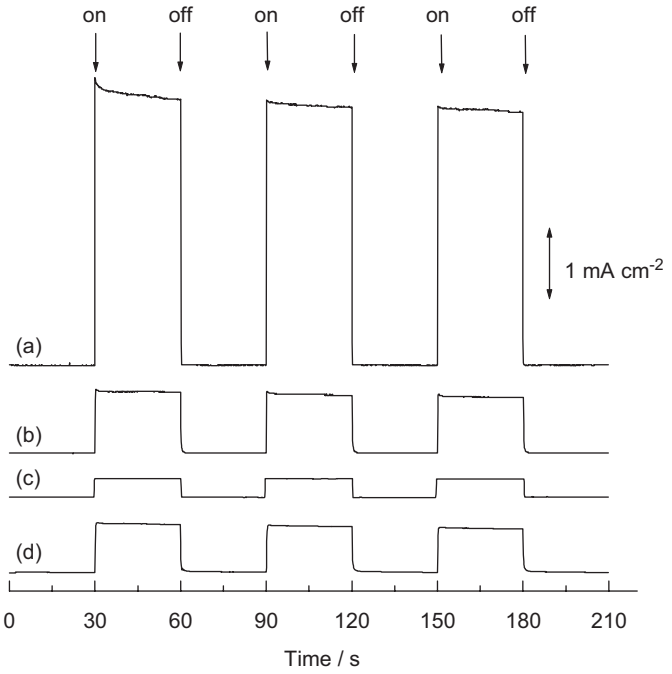

Fig. 8. Time profiles of the photocurrent response by switching irradiation on and off at (a) type-A film, (b) type-B film, (c) type-C film, and (d) type-D film as measured in a 1.0 M $HClO_4$ aqueous solution at 1.2 V vs. SCE. All the films were prepared by calcination at 550 °C.

switching illumination on and off for the type—A–D films are shown in Fig. 8. The photocurrent for the type-A film was 3.7 mA cm^{-2}, which was 4.5–12.8 times higher than those for the others, as summarized in Table 1. It hardly decreased during three times repetition of the illumination switch. The photocurrent is sufficiently maintained during 1 h-steady illumination for the type-A film (12.1% decrease).

The UV–visible DR, XRD spectroscopic and SEM techniques were used to reveal the high catalytic activity of the type-A film. The UV–visible DR spectra are close to each other among type—A–D films, showing that the band gap energy is not considerably different among these films. The XRD data corroborated similar crystallinity of WO_3 for type—B–D films to the type-A film. The SEM data of the surface were measured for type—B–D films to compare with the type-A film in Fig. 3a and b. For the type-B film, the SEM image also exhibited a nano-structured WO_3, but it clumps together (Figure S1 and S2). The surface of the type-C film was observed to be covered with micro-scale

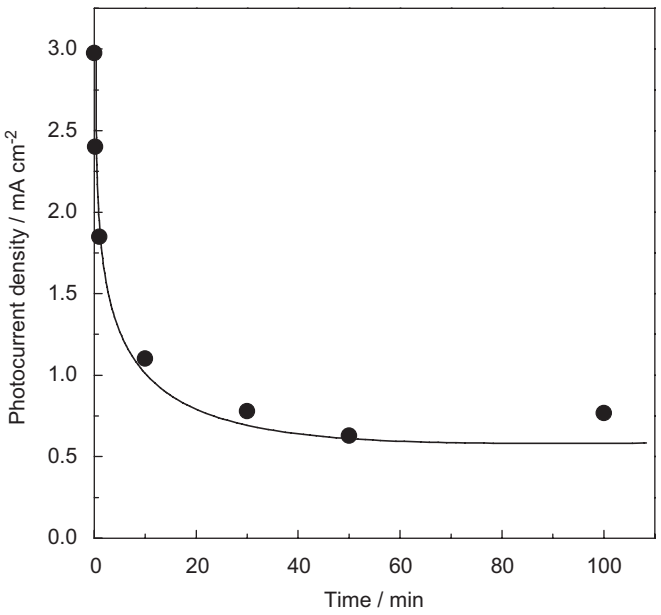

Fig. 9. Plot of the photocurrent vs. time taken for addition of 1.0 ml ethanol for preparation of a precursor solution. The photocurrent was measured in a 1.0 M $HClO_4$ aqueous solution at 1.2 V vs. SCE using the type-A WO_3 film sintered at 550 °C.

plates (Figure S3), and any distinguished nano-structure was not seen in the magnified image shown in Figure S4. For the type-D film, the surface was also observed to be covered with micro-scaled blocks without a distinguished nano-structure (Figure S5 and S6). Thus, the morphology of the type-A film is significantly different from those of type—B–D films. The high catalytic activity of the type-A film could be ascribed to the large interfacial heterojunction area caused by nano-structured WO_3 platelets. It is supported by the higher N_D value for the type-A film than earlier reported WO_3 films. However, there is no guarantee that the catalytic activity is proportional to the interfacial area in the present film.

The comparison of the type-A film with other films points out two technically key procedures for preparation of the nano-structured platelet WO_3 film: (1) preparation of an ammonium tungstate solution by an acid-base reaction of tungstic acid and ammonia solution (comparison with types—B and D), (2) deposition of ammonium tungstate from the solution by the ethanol addition (comparison with type-C). Importance of the deposition by the ethanol addition for the present preparation is especially illustrated by Fig. 9. The photocurrent drastically decreased with time taken for addition of ethanol. The photocurrent decrease was 74% (from 3.0 to 0.78 mA cm^{-2}) when it increased from a few second to 30 min. The quick addition of ethanol is important for the high catalytic activity.

4. Conclusion

A simpler and easier technique was developed for preparation of a WO_3 film composed of nano-structured platelets. The present film produced significant photoanodic current (3.7 mA cm^{-2}) at 1.2 V under illumination with a 500 W xenon lamp. The photocurrent was induced on illumination of UV and visible light below 470 nm, and the maximum IPCE was 47% (1.2 V) at 320 nm. The present a nano-structured platelet WO_3 film could be a promising material to exploit high performance in various photo- and photoelectronic devices available for visible light.

Acknowledgments

This research was partially supported by the joint research project of the Laser Engineering, Osaka University and Grant for Promotion of Niigata University Research Projects. Fellowship grant was provided by The Niigata Engineering Promotion, Inc. (K.S.)

Appendix A. Supplementary materials

Supplementary data associated with this article can bxe found in the online version at doi:10.1016/j.jssc.2007.11.018

Reference

[1] G. Ozin, A. Arsenault, Nanochemistry: A Chemistry Approach to Nanomaterials, Royal Society of Chemistry, London, 2005.
[2] M. Yagi, M. Kaneko, Adv. Polym. Sci. 199 (2006) 143–188.
[3] R. Memming, Semiconductor Electrochemistry, Wiley-VCH, Weinheimk, 2001.
[4] J. Gordon, E. Brown, V.E. Henrich, W.H. Casey, D.L. Clark, C. Eggleston, A. Felmy, D.W. Goodman, M. Graetzel, G. Maciel, M.I. McCarthy, K.H. Nealson, D.A. Sverjensky, M.F. Toney, J.M. Zachara, Chem. Rev. 99 (1999) 77–174.
[5] A.J. Bard, L.R. Faulkner, Electrochemical Methods: Fundamentals, Applications, Wiley, New York, 2001.
[6] A. Fujishima, K. Hashimoto, T. Watanabe, TiO_2 Photocatalysis, Fundamentals and Applications, BKC, Inc., Tokyo, 1999.
[7] B. O'Regan, M. Graetzel, Nature 353 (1991) 737–740.
[8] M. Graetzel, Inorg. Chem. 44 (2005) 6841–6851.
[9] R.J. Colton, A.M. Guzman, J.W. Rabalais, J. Appl. Phys. 49 (1978) 409–416.
[10] B. Yous, S. Robin, A. Donnadieu, G. Dufour, C. Maillot, H. Roulet, C. Senemaud, Mater. Res. Bull. 19 (1984) 1349–1354.
[11] R. Sivakumar, A. Moses Ezhil Raj, B. Subramanian, M. Jayachandran, D.C. Trivedi, C. Sanjeeviraja, Mater. Res. Bull. 39 (2004) 1479–1489.
[12] C. Santato, M. Odziemkowski, M. Ulmann, J. Augustynski, J. Am. Chem. Soc. 123 (2001) 10639–10649.
[13] H. Wang, T. Lindgren, J. He, A. Hagfeldt, S.-E. Lindquist, J. Phys. Chem. B 104 (2000) 5686–5696.
[14] C. Santato, M. Ulmann, J. Augustynski, Adv. Mater. 13 (2001) 511–514.
[15] C. Santato, M. Ulmann, J. Augustynski, J. Phys. Chem. B 105 (2001) 936–940.
[16] K. Yamanaka, H. Oakamoto, H. Kidou, T. Kudo, Jpn. J. Appl. Phys. Part 1 - Regul. Pap. Short Notes Rev. Pap 25 (1986) 1420–1426.
[17] D.L. Bellac, A. Azens, C.G. Granqvist, Appl. Phys. Lett. 66 (1995) 1715–1716.
[18] S.-H. Baeck, K.-S. Choi, T.F. Jaramillo, G.D. Stucky, E.W. McFarland, Adv. Mater. 15 (2003) 1269–1273.
[19] P.K. Shen, A.C.C. Tseung, J. Mater. Chem. 2 (1992) 1141–1147.

[20] M. Yagi, K. Sone, M. Yamada, S. Umemiya, Chem. Eur. J. 11 (2005) 767–775.
[21] M. Yagi, S. Umemiya, J. Phys. Chem. B 106 (2002) 6355–6357.
[22] K. Sone, K. Konishi, M. Yagi, Chem. Eur. J. 12 (2006) 8558–8565.
[23] B.W. Faughnan, R.S. Crandall, M.A. Lampert, Appl. Phys. Lett. 27 (1975) 275–277.
[24] L. Su, Z. Lu, Appl. Spectrosc. 51 (1997) 1587–1590.
[25] L. Su, L. Zhang, J. Fang, M. Xu, Z. Lu, Sol. Energy Mater. 58 (1999) 133–140.
[26] P.S. Patil, P.R. Patil, Sol. Energy Mater. 33 (1994) 293–300.
[27] A. Leaustic, F. Babonneau, J. Livage, J. Phys. Chem. 90 (1986) 4193–4198.